Available online at www.sciencedirect.com
SCIENCE DIRECT®
Journal of Solid State Chemistry 177 (2004) 65–72
JOURNAL OF SOLID STATE CHEMISTRY
http://elsevier.com/locate/jssc

Hexagonal perovskite-intergrowth manganates: $Ln_2Ca_2MnO_7$ (Ln = La, Nd and Sm)

Ying -X. Wang,[a] Li -J. Bie,[a] Yu Du,[a] Jian -H. Lin,[a,*] C.-K. Loong,[b] J.W. Richardson Jr.,[b] and Li -P. You[c]

[a] *The State Key Laboratory of Rare Earth Materials Chemistry and Applications, College of Chemistry and Molecular Engineering, Peking University, Beijing 100871, People's Republic of China*

[b] *Intense Pulsed Neutron Source Division, Argonne National Laboratory, Argonne, IL 60439, USA*

[c] *Electron Microscopy Laboratory, Department of Physics, Peking University, Beijing 100871, People's Republic of China*

Received 10 March 2002; received in revised form 18 June 2002; accepted 30 May 2003

Abstract

Two structures, all consisting of alternative stacking of hexagonal perovskite layer and graphite-like Ca_2O layer, were identified in $Ln_2Ca_2MnO_7$ systems (Ln = La, Nd and Sm). $La_2Ca_2MnO_7$ (1), crystallizing in the space group $R\bar{3}m$ with the lattice constants $a = 5.62231(7)$ Å and $c = 17.3192(4)$ Å, contains almost ideal close packed [LnO_3] arrays. While for the smaller rare earth cations, e.g., $Nd_2Ca_2MnO_7$ (2) and $Sm_2Ca_2MnO_7$ (3), the structure distorts to large unit cell ($R\bar{3}$, $a' = 2a$ and $c' = c$). Study of the substituted systems, $LnLn'Ca_2MnO_7$ (Ln or Ln' = La, Ce, Pr, Nd, Sm, Eu, Gd) and $La_{2-x}Sm_xCa_2MnO_7$, shows a phase transformation from (1) to (2) at certain value of cation size. The MnO_6 octahedra in these compounds are isolated, thus the magnetic property is mainly paramagnetic.

Keywords: Manganate; Hexagonal perovskite-intergrowth; Neutron diffraction; Solid-state structures

1. Introduction

Compounds of perovskite and related structures have been the subjects of interests over several decades, motivated by their remarkable physical properties ranging from high-T_c superconductivity [1,2] to giant magnetoresistivity [3–5]. Among the perovskite-related family, the structural unit of tetragonal perovskite layer, i.e., the (001)-plane of the ideal cubic perovskite [6], is most frequently observed. For example, the Ruddlesden–Popper phase $(ABO_3)_nAO$ [7,8] consists of alternating stacking of n-layered tetragonal perovskite block and single rock-salt-like sheet along the crystallographic c-axis. Intergrowth compounds containing the hexagonal perovskite layer, i.e., the (111)-plane of the ideal cubic perovskite, on the other hand, are rare and less studied. The structural preference to the tetragonal intergrowth clearly originates from the synergistic relationship between the interfacial structures adopted by the perovskite layers and the intergrowth partner components. For example, the cubic perovskite and rock salt structures have identical atomic arrangement in (001) planes with the composition "AO", therefore, the topology of the interfacial structure either remains unchanged or undergoes a minor distortion when they form an intergrowth compound. In contrast, the atomic arrangement on the surface of hexagonal perovskite layer is a close packed [AO_3] array, and a hexagonal intergrowth compound can form only when the insert layer is compatible with this particular structural arrangement at a little energy cost. One of such examples is $Ba_5Ru_2O_{10}$ reported by Grasset et al. [9,10], which consists of alternating 2H-hexagonal perovskite layer [$Ba_3Ru_2O_9$] and graphite-like layer [Ba_2O]. They proposed a hexagonal perovskite series $A_{n+1}M_nO_{3n+3}(A'_2O)$ and attributed $Ba_5Ru_2O_{10}$ as the $n = 2$ member in this family. During a systematic study of the phase diagram of a La–Ca–Mn–O system, we identified a novel manganate $La_2Ca_2MnO_7$ [11,12] that consists of single hexagonal perovskite block [La_2MnO_6] and a graphite-like layer [Ca_2O], hence $n = 1$. In this paper we report the crystal structures of a series compounds $Ln_2Ca_2MnO_7$ (Ln = La, Nd and Sm). The

*Corresponding author. Fax: +86-10-62751708.
E-mail address: jhlin@chem.pku.edu.cn (J.-H. Lin).

0022-4596/03/$ - see front matter © 2003 Elsevier Inc. All rights reserved.
doi:10.1016/S0022-4596(03)00310-4

structural deviation from $La_2Ca_2MnO_7$ in $Nd_2Ca_2MnO_7$ and $Sm_2Ca_2MnO_7$ is attributed to the smaller radii of the rare earth cations. Such trend in this hexagonal perovskite intergrowth series is further verified by a discontinuous change of the lattice constants in the $LnLn'Ca_2MnO_7$ (*Ln* or *Ln*′ = La, Ce, Pr, Nd, Sm, Eu and Gd) and $La_{2-x}Sm_xCa_2MnO_7$ system.

2. Experimental section

All chemicals used in the study were obtained commercially. Purity of the rare earth oxides is 99.99% and alkaline earth and manganese nitrates are all of analytical grade. X-ray powder diffraction patterns (XRD) were recorded by a Rigaku D/Max-2000 diffractometer using Cu$K\alpha$ radiation. The neutron diffraction experiments were carried out using the General Purpose Powder Diffractometer (GPPD) at the Intense Pulsed Neutron Source of Argonne National Laboratory. Electron diffraction studies were carried out using a Hitachi H-9000 electron microscope. The magnetic susceptibility was measured with a SQUID/2000 magnetrometer over the temperature range of about 2 K to room temperature.

2.1. Synthesis of $Ln_2Ca_2MnO_7$ (Ln=La, Nd, Sm) [1–3]

Polycrystalline samples of $Ln_2Ca_2MnO_7$ (*Ln* = La, Nd and Sm) were synthesized by solid-state reaction using the corresponding metal nitrates as starting materials. Citric acid was added to an aqueous solution containing stoichiometric $Ln(NO_3)_3$, $Ca(NO_3)_2$ and $Mn(NO_3)_2$ under stirring. The solution was evaporated on a hot plate to remove water and, the obtained mixture was heated at 600°C in a furnace, producing a fine powder of the mixed oxides. The final products were obtained by heating the mixed oxides at 900°C for 2 days. The mixed rare earth series, $LnLn'Ca_2MnO_7$, where *Ln* or *Ln*′ = La, Pr, Nd, Sm, Eu and Gd, were prepared by similar procedure.

2.2. Crystallographic studies

All of the compounds obtained in this study were in polycrystalline form; therefore, the crystal structures were investigated by powder diffraction techniques. The structures were deduced initially by a direct method and then fully determined by Rietveld refinements of both the neutron and X-ray data.

2.3. Structure refinement of $La_2Ca_2MnO_7$ (1)

The structure of 1 has been reported in the previous report [11] and was described in the space group $R\bar{3}$. Carefully examining the coordinates revealed that the structure could be described in the higher symmetry space group of $R\bar{3}m$. The atomic parameters shown in Table 2 are similar as the previous ones, but this model is more appropriate because fewer variables are needed. The structure refinement with $R\bar{3}m$ structure model resulted in $R_p = 0.061$ and $R_{wp} = 0.082$ for the neutron data and $R_p = 0.069$ and $R_{wp} = 0.098$ for the X-ray data. Fig. 1a shows the profile fit to the neutron diffraction pattern, the crystallographic data are given in Table 1,

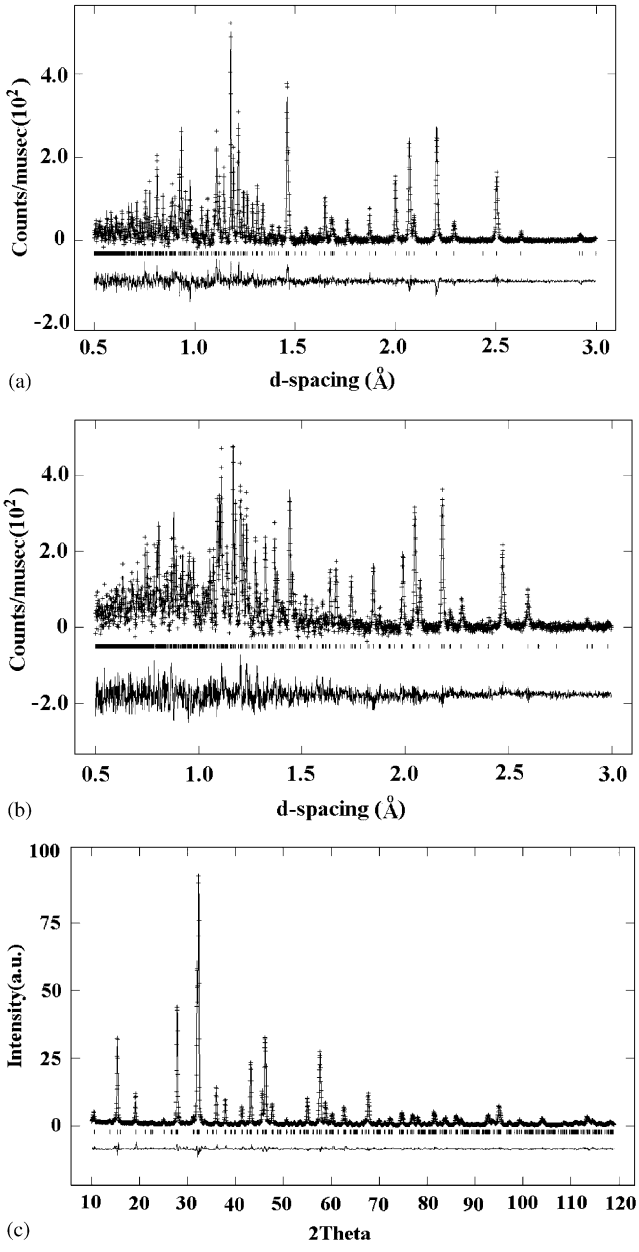

Fig. 1. Profile fit of the neutron powder diffraction pattern of (a) $La_2Ca_2MnO_7$ (1) and (b) $Nd_2Ca_2MnO_7$ (2) and of XRD data of $Sm_2Ca_2MnO_7$ (3). The symbol + represents observed intensity, solid line represents the calculated pattern; the tick marks below the diffraction patterns show the calculated reflection positions, and the residual curve is shown at the bottom of the figure.

Table 1
Crystallographic data of $La_2Ca_2MnO_7$ and $Nd_2Ca_2MnO_7$

		1	2	3
Chemical formula		$La_2Ca_2MnO_7$	$Nd_2Ca_2MnO_7$	$Sm_2Ca_2MnO_7$
Formula weight		524.90	535.57	547.90
Space group		$R\bar{3}m$	$R\bar{3}$	$R\bar{3}$
a (Å)		5.6220(6)	11.1096(2)	11.0441(1)
c (Å)		17.3171(4)	17.1987(9)	17.1300(3)
V (Å^3)		474.0(2)	1838.3(2)	1809.5(1)
Z		3	12	12
ρ_{calcd} (g cm^{-3})		5.517	5.797	5.930
Neutron diffraction data		Collected using General Purpose Powder Diffractometer (GPPD) at the Intense Pulsed Neutron Source of Argonne National Laboratory		
		Room temperature	100 K	Room temperature
X-ray diffraction data		Rigaku D/Max-2000 diffractometer using Cu$K\alpha$ radiation, 50 kV, 100 mA, FT mode, at room temperature		
Structure solution			Direct method (Sirpow92)	
Rietveld refinement			GSAS	
	R_p	0.069	0.086	0.0686
X-ray	R_{wp}	0.098	0.118	0.0993
	R_p	0.061	0.046	
Neutron	R_{wp}	0.082	0.063	

Table 2
Atomic coordinates and isotropic thermal displacement parameters refined with neutron diffraction data of $La_2Ca_2MnO_7$ at room temperature and $Nd_2Ca_2MnO_7$ at 100 K

Atom	Site	x	y	z	U(iso)	Occupation
$La_2Ca_2MnO_7$ (**1**)						
Mn1	3*a*	0	0	0	0.40(9)	1
La1	6*c*	0	0	0.3775(1)	0.42(3)	La/Ca = 0.96/0.04
Ca1	6*c*	0	0	0.8280(2)	0.86(7)	La/Ca = 0.04/0.96
O1	18*h*	0.0146(5)	0.5073(2)	0.6019(1)	1.71(4)	1
O2	18*g*	0	0.126(1)	1/2	1.47(23)	1/6
$Nd_2Ca_2MnO_7$ (**2**)						
Mn1	3*a*	0	0	0	1.61(20)	1
Mn2	9*e*	1/2	0	0	1.61(20)	1
Nd1	6*c*	0	0	0.3773(9)	1.01(7)	Nd/Ca = 0.67/0.33
Nd2	18*f*	0.174(1)	0.339(1)	−0.0435(3)	1.01(7)	Nd/Ca = 0.95/0.05
Ca1	6*c*	0	0	0.176(1)	2.41(16)	Ca/Nd = 0.88/0.12
Ca2	18*f*	0.012(2)	0.506(2)	0.1736(7)	2.41(16)	Ca/Nd = 0.88/0.12
O1	18*f*	0.001(1)	0.183(1)	0.2816(7)	1.46(6)	1
O2	18*f*	0.117(1)	0.153(1)	0.0579(8)	1.46(6)	1
O3	18*f*	0.099(1)	0.664(1)	0.0745(7)	1.46(6)	1
O4	18*f*	0.052(1)	0.388(1)	0.0675(8)	1.46(6)	1
O5	18*f*	0.288(7)	0.686(9)	1/6[a]	0.23(21)	1/6
O6	18*f*	0.254(2)	0.118(2)	1/6[a]	0.23(21)	1/2
$Sm_2Ca_2MnO_7$ (**3**)						
Mn1	3*a*	0	0	0	0.010(20)	1
Mn2	9*e*	1/2	0	0	0.010(20)	1
Sm1	6*c*	0	0	0.3725(3)	0.078(7)	Sm/Ca = 0.67/0.33
Sm2	18*f*	0.1672(5)	0.3314(3)	−0.0435(1)	0.073(7)	Sm/Ca = 0.95/0.05
Ca1	6*c*	0	0	0.1824(5)	0.012(2)	Ca/Sm = 0.88/0.12
Ca2	18*f*	−0.0226(5)	0.484(1)	0.1708(2)	0.012(2)	Ca/Sm = 0.88/0.12
O1	18*f*	0.114(3)	0.161(2)	0.279(1)	0.010[a]	1
O2	18*f*	0.096(3)	0.148(2)	0.063(1)	0.010[a]	1
O3	18*f*	0.091(3)	0.662(3)	0.071(2)	0.010[a]	1
O4	18*f*	0.034(3)	0.374(3)	0.070(2)	0.010[a]	1
O5	18*f*	0.272(5)	0.678(6)	1/6[a]	0.025[a]	1/6[a]
O6	18*f*	0.254(3)	0.123(9)	1/6[a]	0.025[a]	1/2[a]

[a] Refined initially and fixed in the final refinement.

Table 3
Selected bond distances (Å) and angles (degree) in the structure of $La_2Ca_2MnO_7$ at room temperature and $Nd_2Ca_2MnO_7$ at 100 K

$La_2Ca_2MnO_7$ (**1**)			
La1–O1	2.8345(3) × 6	Ca1–O1	2.421(4) × 3
La1–O1	2.536(3) × 3	Ca1–O1	2.380(3) × 3
La1–O2	2.236(3) × 6	Ca1–O2	2.660(6) × 6
Mn1–O1	1.915(2) × 6		
O1–Mn1–O1	89.16(9)	O1–Mn1–O1	90.84(9)
$Nd_2Ca_2MnO_7$ (**2**)			
Mn1–O2	1.835(14) × 6	Nd2–O1	2.870(14)
Mn2–O1	1.711(12) × 2	Nd2–O2	2.530(17)
Mn2–O3	2.040(13) × 2	Nd2–O2	2.397(18)
Mn2–O4	1.984(13) × 2	Nd2–O3	2.571(15)
Nd1–O1	2.408(18) × 3	Nd2–O4	2.545(19)
Nd1–O3	2.632(15) × 3	Nd2–O4	2.432(20)
Nd1–O5	2.167(15)	Nd2–O6	2.285(7)
Nd2–O1	2.594(21)	Nd2–O6	2.246(7)
Ca1–O1	2.527(26) × 3	Ca2–O3	2.230(24)
Ca1–O2	2.555(29) × 3	Ca2–O4	2.477(25)
Ca1–O6	2.458(19)	Ca2–O4	2.248(23)
Ca2–O1	2.560(22)	Ca2–O5	2.80(9)
Ca2–O2	2.524(25)	Ca2–O5	2.55(6)
Ca2–O3	2.286(24)	Ca2–O6	2.75(4)
O2–Mn1–O2	93.4(6)	O1–Mn2–O3	90.5(6)
O2–Mn1–O2	86.6(6)	O1–Mn2–O3	89.5(6)
O1–Mn2–O4	89.1(6)	O3–Mn2–O4	89.4(5)
O3–Mn2–O4	90.6(5)	O3–Mn2–O4	89.4(5)

and the atomic coordinates and selected bond lengths and angles are listed in Tables 2 and 3, respectively.[1]

2.4. Structure determination of $Nd_2Ca_2MnO_7$ (2) and $Sm_2Ca_2MnO_7$ (3)

Structure 2 and 3 was determined with similar procedure as that for 1 [11]. They crystallize also in a rhombohedral structure but with a large unit cells, $a = 11.1096(2)$ Å and $c = 17.1987(9)$ Å for 2 and $a = 11.0441(1)$ Å and $c = 17.1300(3)$ Å for 3, in the space group $R\bar{3}$. The cation positions in the structure were obtained by a direct method [14] and, subsequent Fourier analysis was used to locate the oxygen atoms. The refinement [15] was carried out on both X-ray and neutron diffraction data collected at 100 K for 2 and only on X-ray data for 3. Structure of 2 and 3 is a distorted version of 1, in which the cation sites remain almost unchanged but the oxygen atoms are shifted. Fig. 1 shows the profile fit to the neutron diffraction data for 2 and X-ray data for 3. The crystallographic data, the atomic coordinates and selected bond distances and angles are listed in Tables 1–3, respectively.

[1] During the revision of this paper, Gaudin et al. published a paper concerning about the peroxide ions in $La_2Ca_2MnO_6(O_2)$. They also found that the structure of $La_2Ca_2MnO_7$ is best described in the space group of *R*3*m*. See Ref. [13].

3. Results and discussion

Fig. 2 shows the structure of $La_2Ca_2MnO_7$ (1) projected along (110) direction. The major structural feature of 1 is the stacking of nearly ideal close packed [LaO_3] arrays in the sequence *AABBCC* along the *c*-direction, where the capital letters represent the close packed [LaO_3] at different positions. Alternatively, such a stacking sequence could be viewed as a cubic-closed-packing with a double [LaO_3] layer (*AA*), which generate octahedral and trigonal prismatic sites between the layers, respectively. The manganese and calcium atoms occupying the octahedral and trigonal prismatic sites respectively, and thus forms an intergrowth of a

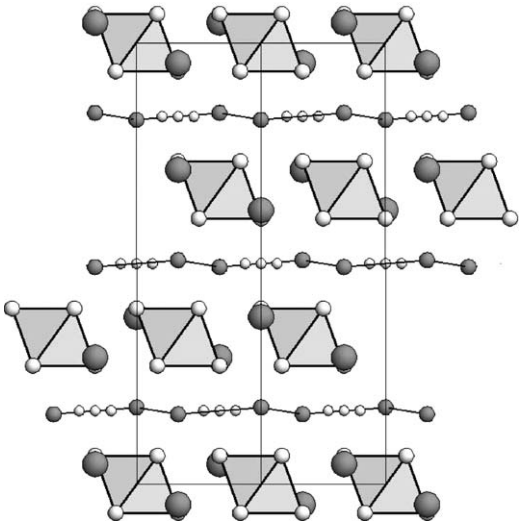

Fig. 2. Projection of the structure of $La_2Ca_2MnO_7$ (1) along (110) direction. Mn1 atoms lie within the octahedra, the vertices are formed by the O1 atoms, La1 atoms are shown as isolated large dark circles. The Ca1 atoms, in the graphite-like network, are shown as small dark circles, and the O2 atoms, described by six-fold distortion, are shown as small light circles.

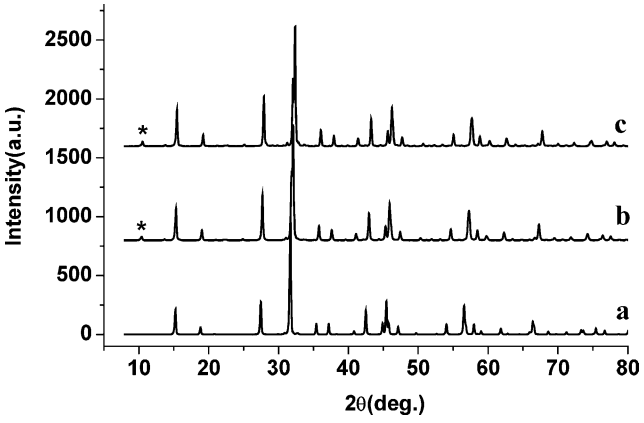

Fig. 3. Powder X-ray diffraction patterns for (a) $La_2Ca_2MnO_7$ (1), (b) $Nd_2Ca_2MnO_7$ (2) and (c) $Sm_2Ca_2MnO_7$ (3). The marks * indicate additional (110) reflection in the distorted structures (2 and 3), which signifies the larger unit cell of the distorted structure.

single-hexagonal-perovskite layer [La_2MnO_6] with a graphite-like layer [Ca_2O]. Note that the lanthanum atoms are located at opposite position in the double [LaO_3] layers, additional oxygen atoms are present around the center of the calcium hexagon. The whole structure can be, therefore, described as alternative stacking of single hexagonal-perovskite [La_2MnO_6] layers and the graphite-like [Ca_2O] layers. According to the structure principle proposed by Grasset et al. [9,10], the structure of $La_2Ca_2MnO_7$ (1) can be assigned as the $n = 1$ member of a hexagonal perovskite-intergrowth family $Ln_{n+1}Mn_nO_{3n+3}(Ca_2O)$, where *Ln* represents rare earth cations.

The $Ln_2Ca_2MnO_7$ compounds for the smaller rare earth cations (*Ln* = Nd and Sm) are distorted derivatives of 1. The X-ray diffraction patterns are rather similar for all three compounds (Fig. 3), except that several additional weak reflections appear in 2 and 3, due to structure distortion. Fig. 4 shows the electron diffraction patterns in the [010] and [$\bar{1}10$] zones for 1 and 2. Both show typical rhombohedral diffraction patterns. The main diffraction spots in both patterns are similar and can be indexed with a rhombohedral cell $a \approx 5.6$ Å and $c \approx 17.3$ Å. For compound 2, however, additional weak super-reflections are present, indicating the doubling of the *a*-axis. The extra peaks in the diffraction pattern can be indexed with a large rhombohedral cell $a' \approx 2a$ and $c' \approx c$.

The distortions in the structure of 2 and 3 arise mainly due to the smaller size of the *Ln* cations relative to La, whereby the [LnO_3] layers are no longer ideal close-packed arrays but distorted. The coordination

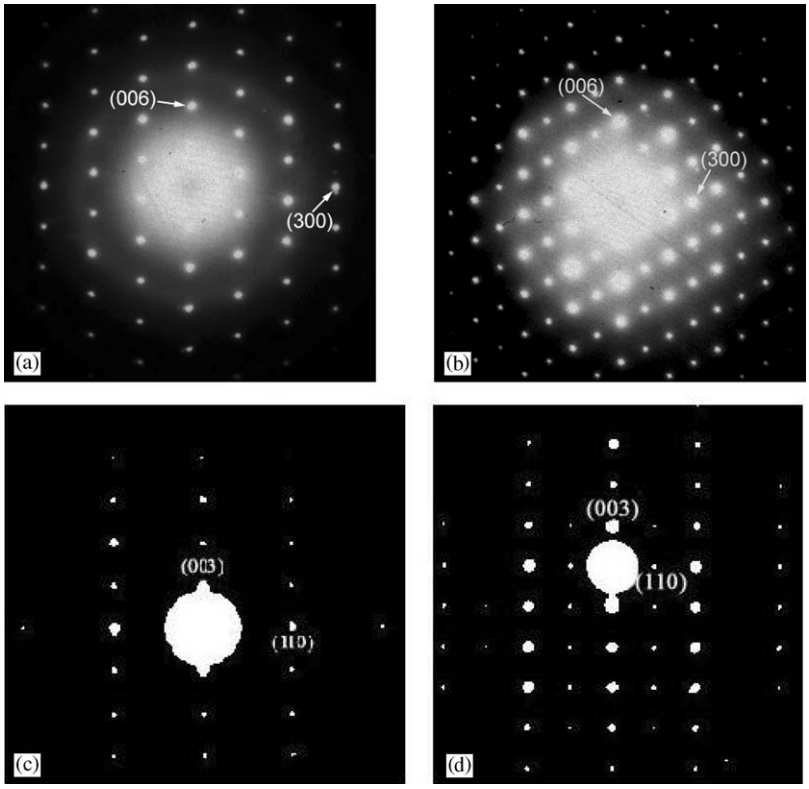

Fig. 4. Electron diffraction patterns in the [010] zone for (a) $La_2Ca_2MnO_7$ and (b) $Nd_2Ca_2MnO_7$ and, in the [$\bar{1}10$] zone for (c) $La_2Ca_2MnO_7$ and (d) $La_2Ca_2MnO_7$. The additional weak super-reflections in (b) and (d) originate from the structural distortion that leads to the doubling of the unit cell *a*-axis.

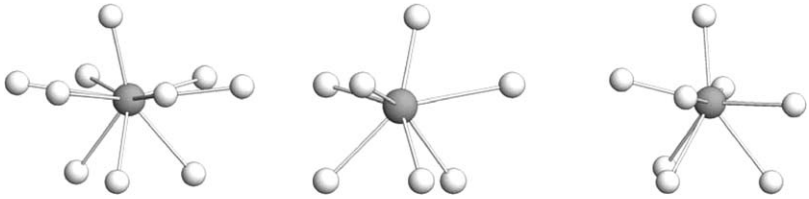

Fig. 5. Coordination polyhedra for (a) La1 in $La_2Ca_2MnO_7$ (1), (b) Nd1 and (c) Nd2 in $Nd_2Ca_2MnO_7$ (2).

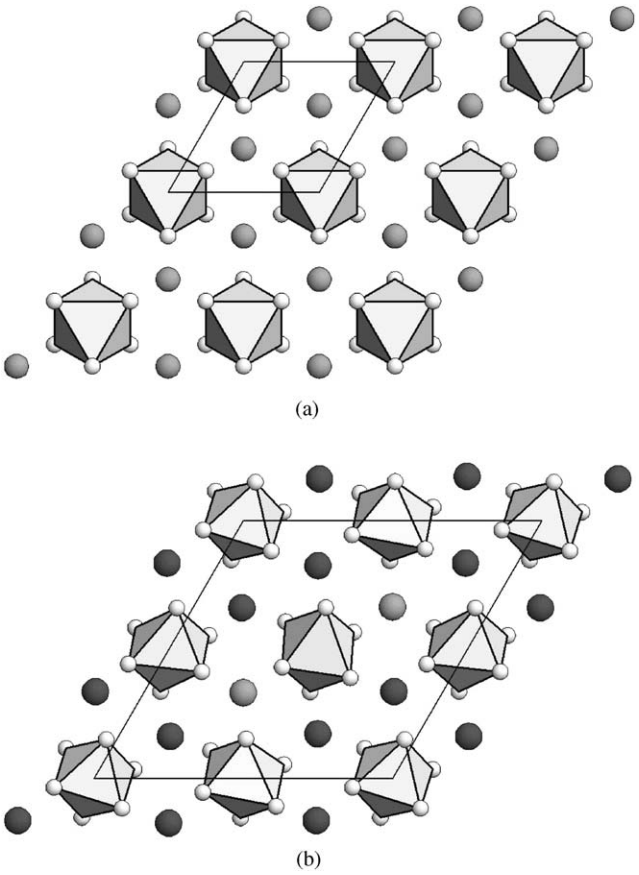

Fig. 6. Hexagonal perovskite layer in (a) $La_2Ca_2MnO_7$ (1) and (b) $Nd_2Ca_2MnO_7$ (2).

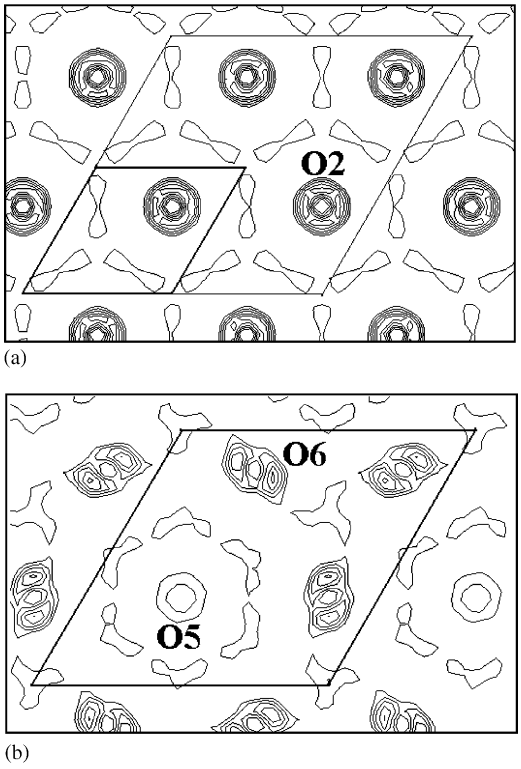

Fig. 7. Difference Fourier map at the section of the $[Ca_2O]$ layer for (a) $La_2Ca_2MnO_7$ (1) and (b) $Nd_2Ca_2MnO_7$ (2), calculated by including all atoms except the oxygen atoms in the graphite-like layer $[Ca_2O]$.

polyhedra of the rare earth cations are, therefore, significantly different as shown in Fig. 5. The La1 atom in 1 is surrounded by 10 oxygen atoms (Fig. 5a), nine of which, i.e., O1, have the bond distances of 2.536 Å and 2.835 Å, and the O2 in the $[Ca_2O]$ layer, showing a six-fold distortion, bonds more closely to La (2.236 Å). In structure 2, the Nd atoms occupy two crystallographic independent positions and, the oxygen atoms are shifted, resulting in a low coordination number to the Nd atoms. The Nd1 is surrounded by seven oxygen atoms with the bond distances ranging from 2.167 to 2.632 Å and the Nd2 is coordinated by eight oxygen atoms from 2.246 to 2.870 Å. In Fig. 6, we compare the single hexagonal-perovskite layers $[Ln_2MnO_6]$ in both structures. The hexagonal-perovskite layer is almost ideal in 1, while the rotation of the MnO_6 octahedra is apparent in structure 2, although the local coordination of manganese atoms is rather regular as indicated by the bond lengths and angles in Table 2.

The oxygen atoms in the graphite-like Ca_2O layers are located in a hexagonal-bipyramidal polyhedron. The distance between the opposite *Ln* atoms is about 4.2 Å in 1, which is too short for an oxygen to be located at the center of the hexagon. In both structures, the oxygen positions are shifted from the center. Fig. 7 shows the difference Fourier maps at the section of the $[Ca_2O]$ layer for both 1 and 2 that represents the distribution of the oxygen atoms in $[Ca_2O]$. In the structure 1, the oxygen atom (O2) is located symmetrically around the center of the Ca-hexagon and is described by a partially occupied (1/6) special position (18*g*) within the space group $R\bar{3}m$. The two oxygen atoms (O5 and O6) in structure 2 are distributed in different fashions (Fig. 7b). The O5 is located symmetrically around the three-fold axis and is partially occupied (1/6) at 18f, while the O6 is located at 18f with a two-fold distortion (1/2).

Two factors may influence the formation of the $Ln_2Ca_2MnO_7$ phases. Firstly, only the rare earth cations larger than Eu can form these compounds. Thus the smallest rare earth that can form this phase is samarium and the other smaller rare earth systems only let to simple perovskite-type phases and other known binary oxides. Secondly the high valence rare earth cations (IV) is unfavorable. Therefore, $Ce_2Ca_2MnO_7$ does not present and, although $Pr_2Ca_2MnO_7$ has been identified, it always contains considerable amount of impurity due to partial oxidation of Pr (III) to Pr(IV).

In order to study the influence of cation size on the structure, we synthesized several systems $LnLn'Ca_2MnO_7$, where *Ln* and $Ln' =$ La, Ce, Pr, Nd, Sm, Eu and Gd. In these systems, the effective cation size varies. Fig. 8a shows the dependence of the lattice constants on

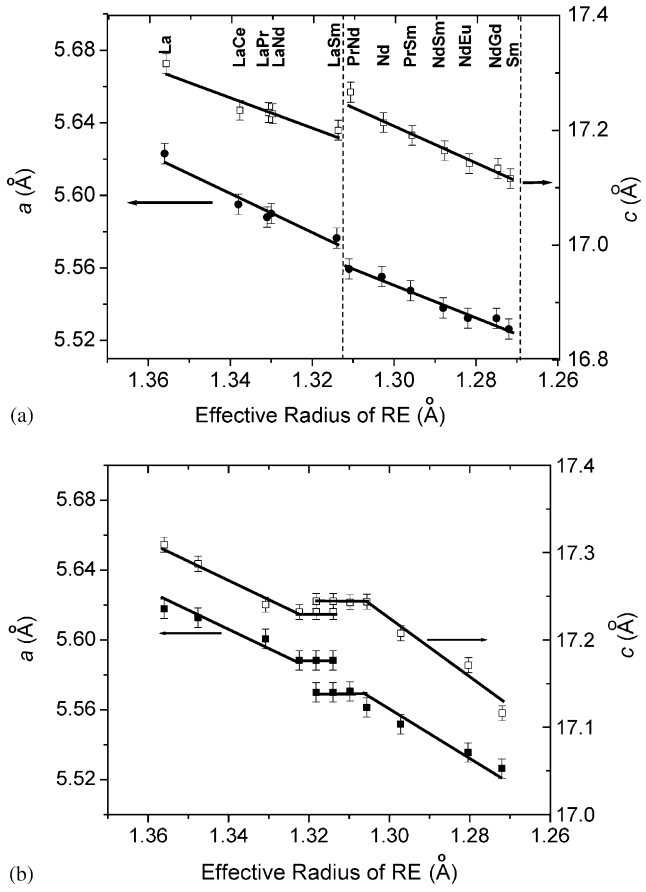

Fig. 8. (a) Variation of the lattice constants normalized to structure 1 with respect to the effective radii of rare earth cations in the $LnLn'Ca_2MnO_7$ system. The boundary shown as dotted lines separate the undistorted/distorted phases ($R=1.31$ Å) and the phase boundary ($R=1.27$ Å) of the $LnLn'Ca_2MnO_7$ system. (b) Variation of the lattice constants normalized to structure 1 with respect to the effective radii of rare earth cations in the $La_{2-x}Sm_xCa_2MnO_7$ system. A two-phase region between the two structure forms can be seen around $R=1.31$–1.32 Å.

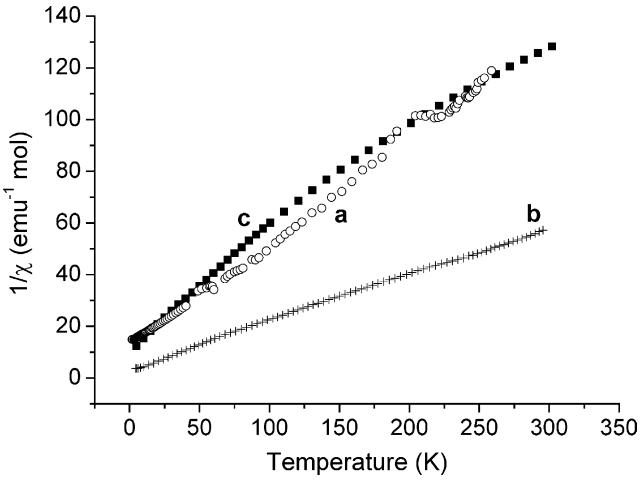

Fig. 9. The inverse magnetic susceptibility of (a) $La_2Ca_2MnO_7$, (b) $Nd_2Ca_2MnO_7$ and (c) $Sm_2Ca_2MnO_7$ versus temperature.

the effective cation radii in the $LnLn'Ca_2MnO_7$ system. It can be seen that the $Ln_2Ca_2MnO_7$ phases are formed as long as the effective cation size is larger than 1.27 Å. The phase diagram can be divided into two regions, respectively in $La_2Ca_2MnO_7$ and $Nd_2Ca_2MnO_7$ structure types. Within each region the lattice constants vary continuously. But a discontinuous change occurs at $LaSmCa_2MnO_7$/$PrNdCa_2MnO_7$ represented by a sudden increase of the c and a decrease of the a parameter. The critical value of effective radius is about $R\approx1.31$ Å. Larger cations ($R>1.31$ Å) form $La_2Ca_2MnO_7$ structure and smaller cations ($R<1.31$ Å) form distorted structure of the $Nd_2Ca_2MnO_7$ type. Thus diagram represents the dependence of the structure distortion on the effective cation radii of the rare earth cations. In addition, Ce can partially substitute La forming $LaCeCa_2MnO_7$ although $Ce_2Ca_2MnO_7$ itself does not present.

To follow the phase transition more closely, another series $La_{2-x}Sm_xCa_2MnO_7$ samples were prepared. As shown in Fig. 8b, the variation of the lattice constants in the $La_{2-x}Sm_xCa_2MnO_7$ system shows a similar behavior as $LnLn'Ca_2MnO_7$. However, a two-phase region can be clearly seen in the region of $1.305<R<1.315$ Å. Within the two-phase region, the lattice constants were determined by using Rietveld refinement of structures including both phases. The hexagonal perovskite layers in the $La_2Ca_2MnO_7$ type is almost ideal. As the rare earth cation size decreases, an internal stress builds up in the crystal lattice, and at certain value the ideal hexagonal perovskite layer becomes unstable, and a collective distortion of the lattice occurs to release the internal stress. Such distortion leads to a contraction within the $a-b$ plane and expansion along the c-axis in order to satisfy the coordination requirement for the smaller rare earth cations.

In all of these compounds, the MnO_6 octahedra in hexagonal perovskite layers are isolated; therefore, one expects a localized magnetic behavior. Fig. 9 shows the inverse of the magnetic susceptibility for $La_2Ca_2MnO_7$ (1), $Nd_2Ca_2MnO_7$ (2) and $Sm_2Ca_2MnO_7$ (3). All of them exhibit Curie–Weiss behavior down to low temperatures with a Weiss constant of $\theta=36.4$, 13.4 and 23.3 K, respectively.

In conclusion, the hexagonal perovskite-intergrowth compounds $Ln_2Ca_2MnO_7$ were found for $Ln=$ La, Nd and Sm, and the fundamental structure is described as alternative stacking of single hexagonal perovskite layer [La_2MnO_6] and the graphite-like layer [Ca_2O], hence an $n=1$ member in the $Ln_{n+1}Mn_nO_{3n+3}(Ca_2O)$ family. For the smaller rare earth cations, such as Nd and Sm, the structure is distorted to a lower symmetry with a larger unit cell. The phase transformation is mainly due to decrease of the rare earth cation size, which induces structure distortion of the close packed [LnO_3] array in order to meet the coordination requirement for the smaller rare earth cations. Thus the structural distortion

and the lattice constants exhibit correlation to the effective cation size in $LnLn'Ca_2MnO_7$ (Ln or $Ln' = La$, Ce, Pr, Nd, Sm, Eu and Gd) and $La_{2-x}Sm_xCa_2MnO_7$ systems.

Acknowledgments

We are thankful to the financial support from NSFC (20221101) and the State Key Basic Research Program. Work performed at Argonne is supported by US DOE-BES under Contract No. W-31-109-ENG-38.

References

[1] J.G. Bednorz, K.A. Muller, Z. Phys. B 64 (1986) 189.
[2] J.P. Attfield, A.L. Kharlanov, J.A. McAllister, Nature 394 (1998) 157.
[3] R. von Helmolt, J. Wecker, B. Holzapfel, L. Schultz, K. Sanwer, Phys. Rev. Lett. 71 (1993) 2331.
[4] B. Raveau, A. Maignan, C. Martin, M. Hervieu, Chem. Mater. 10 (1998) 2641.
[5] C.N.R. Rao, A. Arulraj, P.N. Santosh, A.K. Cheetham, Chem. Mater. 10 (1998) 2714.
[6] G.B. Hyde, S. Andersson, Inorganic Crystal Structures, Wiley, New York, 1989.
[7] C.N.R. Rao, B. Raveau, Transition Metal Oxides, 2nd Edition, Wiley-VCH, New York, 1998, p. 61.
[8] P.D. Battle, W.R. Branford, A. Mihut, M.J. Rosseinsky, J. Singleton, J. Sloan, L.E. Spring, J.F. Vente, Chem. Mater. 11 (1999) 674.
[9] F. Grasset, C. Dussarrat, J. Darriet, J. Mater. Chem. 7 (1997) 1911.
[10] F. Grasset, M. Zakhour, J. Darriet, J. Alloys Compds. 287 (1999) 25.
[11] Y.X. Wang, J.H. Lin, Y. Du, R.W. Qin, B. Han, C.K. Loong, Angew. Chem. 112 (2000) 2842; Angew. Chem. Int. Ed. 39 (2000) 2739
[12] Y.X. Wang, Y. Du, R.W. Qin, B. Han, J.H. Lin, J. Solid State Chem. 156 (2000) 237.
[13] E. Gautin, G. Goglio, A. Besnard, J. Darriet, J. Solid State Chem., in press, available online 8 April 2003.
[14] A. Altomare, M.C. Burla, M. Camalli, G. Cascarano, C. Giacovazzo, A. Guagliardi, G. Polidori, J. Appl. Cryst. 27 (1994) 435.
[15] A.C. Larson, R.B. von Dreele, Report LAUR 86-748, Los Alamos National Laboratory, 1985.